Graded porous scaffold mediates internal fluidic environment for 3D *in vitro* mechanobiology

Chiara Angela De Rosa [a,b], Christopher J. Wright [a], Yi Xiong [c], Francesco Del Giudice [d], Feihu Zhao [a,b,*]

[a] *Department of Biomedical Engineering, Faculty of Science and Engineering, Swansea University, Swansea, United Kingdom*
[b] *Zienkiewicz Institute for Modelling Data and AI, Swansea University, Swansea, United Kingdom*
[c] *School of System Design and Intelligent Manufacturing, Southern University of Science and Technology, Shenzhen, Guangdong Province, China*
[d] *Complex Fluid Research Group, Department of Chemical Engineering, Faculty of Science and Engineering, Swansea University, Swansea, United Kingdom*

ARTICLE INFO

ABSTRACT

Most cell types are mechanosensitive, their activities such as differentiation, proliferation and apoptosis, can be influenced by the mechanical environment through mechanical stimulation. In three dimensional (3D) mechanobiological *in vitro* studies, the porous structure of scaffold controls the local mechanical environment that applied to cells. Many previous studies have focused on the topological design of homogeneous scaffold struts. However, the impact of scaffold inhomogeneity on the mechanical environment, which is essential in mechanobiological application (e.g. for multi-cells co-culture), remains elusive. In this study, we use a computational fluid dynamics (CFD) approach together with data analysis to study the influence of a porosity gradient (10 %–30 % porosity difference) on the local and global mechanical environment (wall shear stress - WSS) within the commonly used structures of triple periodic minimal surfaces (TPMS). In addition, the anisotropy of internal WSS and scaffold permeability caused by the porosity gradient is investigated. It is found that the influence of anisotropy on the average WSS and permeability is up to 11 % and 31 %, respectively. These results, as theoretical references will be useful to tissue engineers and mechanobiologists for scaffold design and *in vitro* experiment planning such as integrated use of graded scaffold and bioreactors for specific cell types.

1. Introduction

Most cells are mechanosensitive, meaning their activities can be influenced by the mechanical environment (i.e., mechanical stimulation). Therefore, the mechanical environment is important for *in vitro* mechanobiological studies, which provide significant insight to guide functional tissue regeneration for tissues such as bone and cartilage [1, 2]. Among the different types of mechanical stimulation, fluid-induced wall shear stress (WSS) is commonly used for stimulating the cells, in particular stem cells, bone cells and endothelial cells [3]. WSS is the force per unit area in a plane tangential to the cell walls. For instance, it was found that the WSS in the range of 0.55 mPa–10 mPa can stimulate mesenchymal stem cells (MSCs) to differentiate towards an osteogenic lineage and produce mineralized matrix during *in vitro* bone tissue engineering [4]. For endothelial cells (ECs) mechanobiology, it was reported that a WSS of 0.2 Pa can stimulate ECs realignment, and cause

rapid conformational activation of integrin $\alpha_v\beta_3$ [5].

In three dimensional (3D) mechanobiological experiments, porous scaffolds are usually used for housing the cells. The cell-seeded scaffolds are then placed in a bioreactor/fluidic device, which generates fluid-induced WSS on cells [6]. It has been reported that to control the WSS on cells, researchers need to either tune the bioreactor mechanical loading (such as applied flow rate) or control the scaffold micro-porous geometries [7]. However, the geometry of a scaffold has numerous possibilities, which raises the time and computational cost for scaffold design. In recent studies, scaffolds with Triply Periodic Minimal Surfaces (TPMS) topology have gained much attention due to their advantages that includes a high surface area to volume ratio, less stress concentration, and increased permeability compared to the traditional lattice structures, thereby aiding better cell adhesion, migration, and proliferation [8–10]. Most of the current studies for scaffold design have been focused on scaffolds with homogenous pores, which can result in
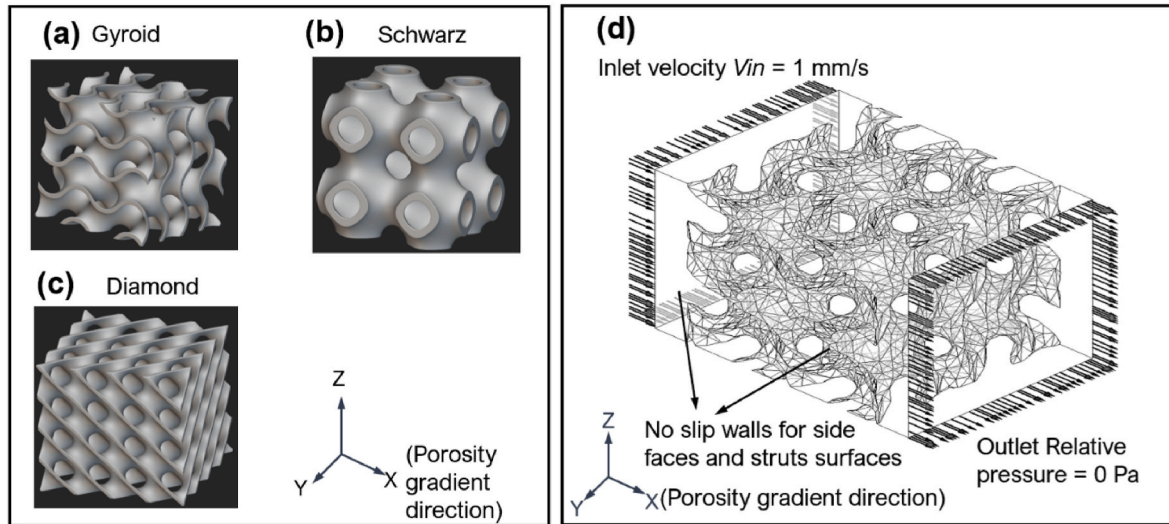

Fig. 1. Scaffolds with TPMS geometries, i.e., **(a)** gyroid, **(b)** Schwarz, **(c)** diamond; **(d)** boundary and loading conditions of the CFD model. Porosity gradient is in the X-direction.

homogeneous distribution of the mechanical stimulation throughout the scaffold within a perfusion bioreactor/fluidic device [11]; [12]. To generate different mechanical stimulation in different regions of scaffolds, the local geometric features will need to be tuned [13]. For example, within a perfusion bioreactor, the scaffold section with higher porosity results in a lower WSS compared to the one with lower porosity [14]. In some applications for multi-cells co-culture, cells in different regions within a scaffold with graded porosity can experience different levels of mechanical stimulation. Therefore, to accurately generate a controlled local mechanical environment within different regions of a scaffold, by tuning the local scaffold geometric features (such as porosity and pore size), it is essential to comprehensively understand the explicit influence of porous geometry gradients on the generated mechanical environment within the scaffold. However, such quantitative influence has not been extensively investigated.

In this study, characterization of the impact of scaffold inhomogeneity on the micro-mechanical environment is performed. To do this, scaffolds with three types of TPMS structures (gyroid, Schwarz and diamond shapes), which have different porosity gradients (between 60 % and 90 %) are created, and simulated with a computational fluid dynamics (CFD) approach for an application scenario based on a perfusion bioreactor/fluidic device. Furthermore, the generated WSS and permeability influenced by the porosity gradient are quantitatively analyzed. The output from this study will provide a quantitative reference for scaffold design and the application of fluidic devices in 3D mechanobiological studies, in particular for multi-cells co-culture.

2. Methods

2.1. Scaffold porous geometry generation

To generate the scaffold geometries for CFD simulation, the computer-aided design (CAD) software, nTopology (nTopology Inc, NY, USA) was used. In this study, three types of commonly used TPMS structures were used. These were gyroid, Schwarz and diamond structures as shown in Fig. 1(a–c). The governing equation of the three topologies are as Eqs. (1)–(3) [15]:

$$U_G = cos(k_x x)sin(k_y y) + cos(k_y y)sin(k_z z) + cos(k_z z)sin(k_x x) - t \tag{1}$$

$$U_S = cos(k_x x) + cos(k_y y) + cos(k_z z) - t \tag{2}$$

Table 1
Geometric details of TPMS scaffolds that have different porosity gradients.

	Porosity	Minimum Wall Thickness [mm]	Maximum Wall Thickness [mm]
Gyroid	90-80 %	0.15	0.31
	80-70 %	0.31	0.46
	70-60 %	0.46	0.62
	90-70 %	0.15	0.46
	80-60 %	0.31	0.62
	90-60 %	0.15	0.62
Schwarz	90-80 %	0.09	0.18
	80-70 %	0.18	0.26
	70-60 %	0.26	0.35
	90-70 %	0.09	0.26
	80-60 %	0.18	0.35
	90-60 %	0.09	0.35
Diamond	90-80 %	0.13	0.26
	80-70 %	0.26	0.40
	70-60 %	0.40	0.51
	90-70 %	0.13	0.40
	80-60 %	0.26	0.51
	90-60 %	0.13	0.51

$$U_D = sin(k_x x)sin(k_y y)sin(k_z z) + sin(k_x x)cos(k_y y)cos(k_z z) \\ + cos(k_x x)sin(k_y y)cos(k_z z) + cos(k_x x)cos(k_y y)sin(k_z z) - t \tag{3}$$

where, U_G, U_S, $U_D = 0$ are for the isosurface of gyroid, Schwarz and diamond structures, respectively; NTopology uses this isosurface as the boundary between solid and void material phases; t is a variable to control the volume fraction; k_i are the TPMS function periodicities, defined as Eq. (4):

$$k_i = 2\pi \frac{n_i}{L_i} \ (with \ i = x, y, z) \tag{4}$$

where, n_i are the number of cell repetitions in the directions of x, y and z, L_i are the overall dimensions of the structure in those directions.

Based on these strut topologies, different porosity gradients (in Table 1) were applied to generate the graded scaffolds. In this study, porosity is the ratio between the volume of void (i.e., porous space within scaffold) and the total volume of scaffold. Porosity gradient is the porosity difference across the entire scaffold (i.e., X-axis direction).
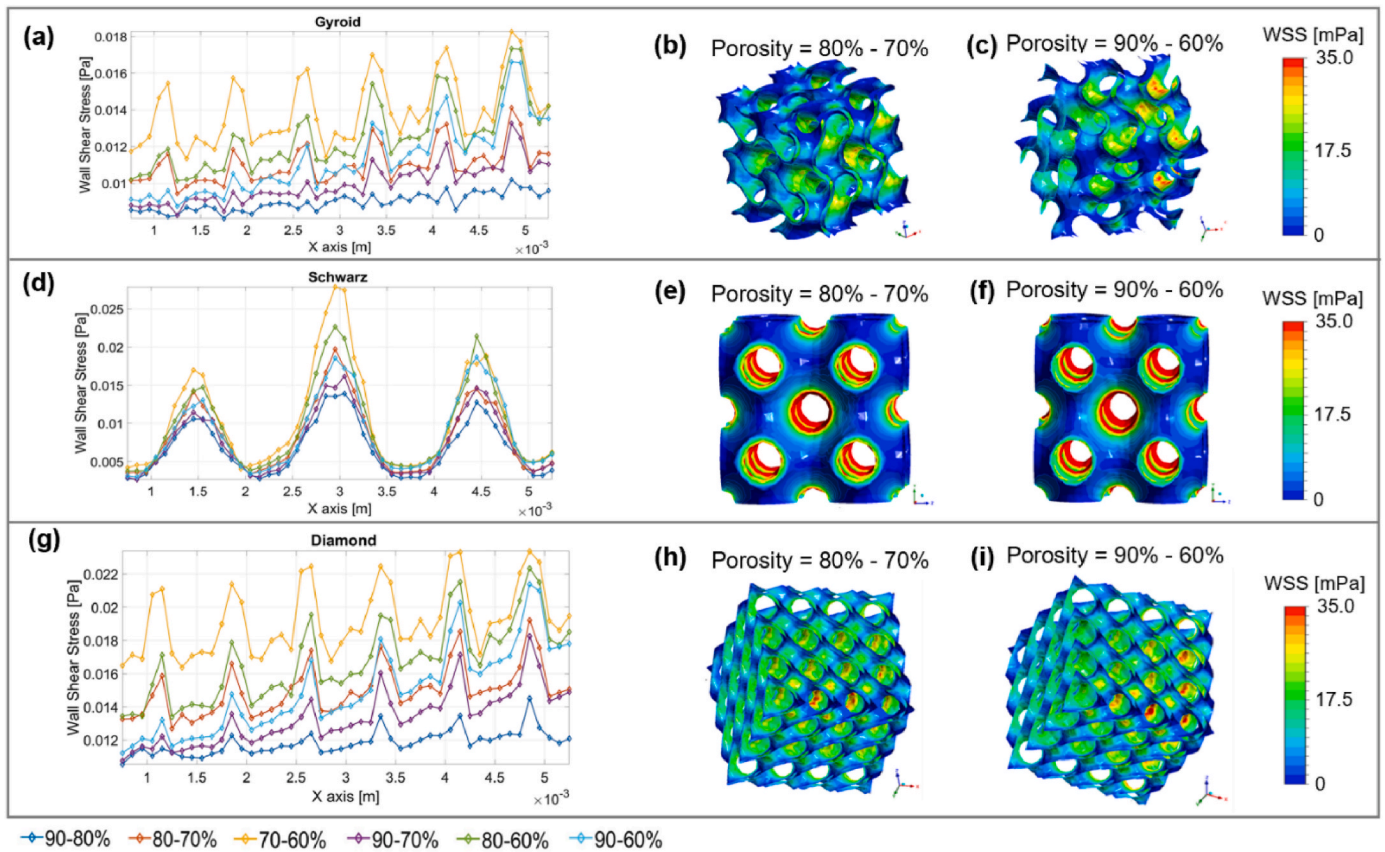
Fig. 2. WSS in the direction of porosity gradient (x axis) within the graded scaffolds with **(a - c)** gyroid, **(d - f)** Schwarz and **(g–i)** diamond struts under the perfusion flow parallel to the direction of porosity gradient.

2.2. CFD simulation

To quantify the fluid-induced WSS and permeability influenced by scaffolds' graded porosities, a CFD approach was used. Considering the perfusion bioreactor conditions, an inlet fluid velocity of 1.0 mm/s and outlet pressure of 0 Pa (relative to air pressure) were applied according to the suggestion for *in vitro* bone tissue engineering from previous study by Zhao et al. [16]. The side faces and internal strut surfaces were defined as non-slip walls (Fig. 1d), where fluid velocity is zero. To investigate the influence of anisotropy of porosity gradient, the inlet – outlet was applied parallel and perpendicular to the direction of the porosity gradient. After mesh sensitivity analysis, the CFD domain of all geometries were meshed with a global element size of 0.08 mm. Moreover, the local mesh size was refined automatically according to curvature features of the geometries; the maximum allowable angle that one element edge could span another was 18°. This resulted in approximately 2 million tetrahedral elements for each CFD model geometry based on a patch conforming method. In the CFD model, the Navier-Stokes equation (Eq. (5)) was solved by a finite volume method (FVM) using the commercial solver – ANSYS CFX (ANSYS Inc., PA, USA) under the convergence criteria of the root mean square residual of the mass and momentum $< 10^{-5}$. The flow was defined as laminar, as the Reynold's number (Re) < 10 for cases in this study according to the pre-computation.

$$\begin{cases} \nabla \bullet \mathbf{v} = 0 \\ \rho \left(\dfrac{\partial \mathbf{v}}{\partial t} + \mathbf{v} \bullet \nabla \mathbf{v} \right) = -\nabla p + \mu \nabla^2 \mathbf{v} \end{cases} \tag{5}$$

where, $\mathbf{v}$ is the fluid velocity vector; ρ is the fluid density (i.e., for water $\rho = 1000 \text{ kg/m}^3$); μ is the fluid dynamic viscosity (i.e., for water $\mu = 0.89 \text{ mPa} \bullet \text{s}$).

The WSS on the struts surfaces was calculated according to Eq. (6):

$$\tau = \mu \bullet \left(\frac{\delta v_i}{\delta x_j} + \frac{\delta v_j}{\delta x_i} \right) \bigg|_{x_i \in \Gamma s} \tag{6}$$

where, x_i (or x_j) is the ith (or jth) spatial coordinates; Γs represents the boundary of struts surfaces.

Permeability is a parameter that can influence the nutrient delivery within the scaffolds [17,18]. Therefore, in this study, permeability of different scaffold designs are calculated using Darcy's law Eq. (7):

$$\kappa = \frac{\mu q L_i}{\Delta p} \tag{7}$$

where, κ is the scaffold permeability; q is the Darcy velocity; L_i is the overall length of the scaffold; Δp is the pressure drop over the scaffold, which is calculated from CFD model above.

Moreover, the anisotropic property of permeability due to the graded porosity is assessed in the directions of parallel and perpendicular to the porosity gradient.

2.3. Data analysis

To study the influence of the porosity gradient on the local WSS under different directions of perfusion flow, the WSS data on 3D strut surfaces (Γs) was collected, and re-processed into 1D (i.e., in porosity gradient direction) in Matlab (Mathworks Inc., CA, USA). WSS on the nodes of each element were sorted and discretized along the porosity gradient direction (i.e., x-direction in Fig. 1d) with an interval of 0.1 mm, then the average value of WSS was calculated for each interval slot in x-direction. Considering the convenience in future application (e.g., any potential user can easily estimate the local WSS) and the accuracy of
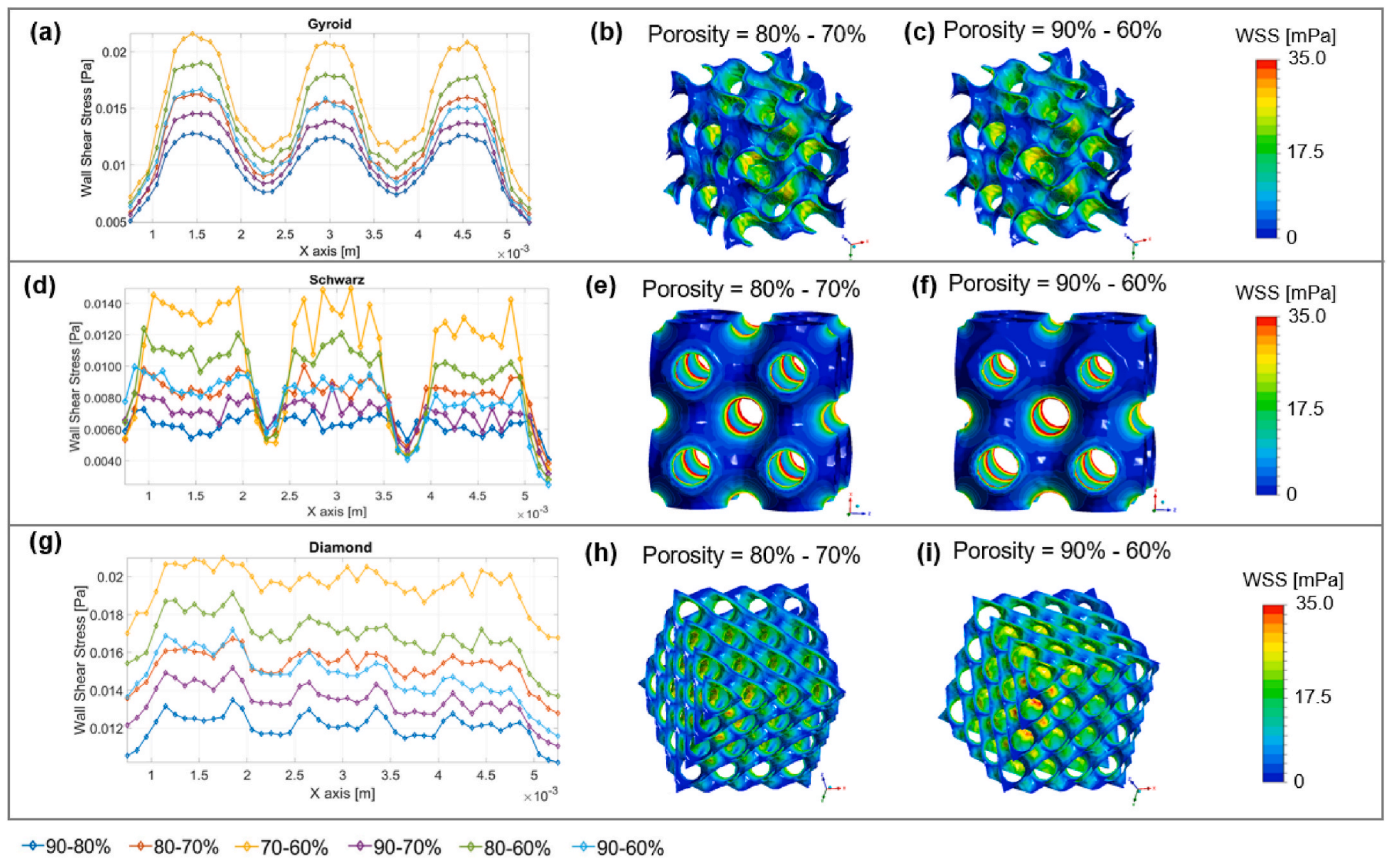
Fig. 3. WSS in the direction of porosity gradient (x axis) within the graded scaffolds with **(a - c)** gyroid, **(d - f)** Schwarz and **(g–i)** diamond struts under the perfusion flow perpendicular to the direction of porosity gradient.

the data fitting, linear regression analysis was used for finding the expressions of location-dependent WSS influenced by the porosity gradient.

3. Results and discussion

3.1. WSS distribution and permeability

The CFD simulation results show that the gyroid and Schwarz shapes have distinct anomalies of WSS distribution along the x direction, the direction of porosity gradient, while this is less obvious for the diamond shape scenario under both flow directions, parallel and perpendicular to x direction as shown in Figs. 2 and 3. Many previous studies have reported the phenomenon of strut topology – influenced internal WSS [7, 9]. Therefore, the WSS change along the x direction could be attributed to the influence from the struts surface shape as described in eqs. (1)–(3). Under flow in a parallel direction to the porosity gradient, the scaffolds with Schwarz structure have larger WSS variation throughout the scaffold and higher WSS concentration, compared to gyroid and diamond structures (Fig. 2). However, the influence of porosity gradient on the WSS variation is more obvious for diamond structures under either parallel or perpendicular flow, the lines are sparser for diamond structures in Fig. 2g and 3g. Therefore, this means that the scaffold with diamond-shaped struts will be a good option to minimize the influence of local strut topology while maximizing the influence of the porosity gradient. In terms of WSS within scaffolds, the strut topology shows distinct influence on the overall average WSS within scaffolds (Fig. 4a). The corresponding maximum and minimum WSS can be found in Supplementary Material - Supplementary Table 1. The scaffolds with diamond struts result in higher average WSS within the scaffolds than gyroid and Schwarz struts under the same porosity gradient.

After fitting the data (as shown in Figs. 2 and 3 a, b and g), the specific expression of the local WSS with respect to x (porosity gradient direction) for all the scaffolds in this study were obtained as below:

$$\tau = p_1 \bullet x + p_2 \qquad (8)$$

where, p_1 and p_2 are coefficients by fitting the data as shown in Table 2.

An example of data fitting for scaffolds with the graded porosity of 90 %–60 % is shown in the Supplementary Material - Supplementary Fig. 1. Comparing the scaffolds with graded porosity to the ones with homogeneous porosity, although the local WSS still has anomalies within homogeneous scaffolds, the peak and bottom values of WSS within each scaffold are consistent along X-direction, i.e., $p_1 = 0$ (Supplementary Material - Supplementary Fig. 2), while $p_1 \neq 0$ for the scaffolds with graded porosity (see Table 2). Moreover, it is found that higher porosity gradient results in a higher influence on WSS, according to p_1 values in Table 2. The porosity gradient has more distinct influence on the WSS in scaffolds with gyroid and diamond strut topology than scaffolds with Schwarz strut topology. Other studies have found that pore size also influences the resultant WSS within scaffold [7,9]. Considering the manufacturing, precisely controlling the porosity is easier/more feasible than controlling pore size, in particular for conventional technique, such as salt leaching [19]. Therefore, this study is focused on the porosity of graded scaffolds. For the flow perpendicular to the porosity gradient, the diamond strut topology has more obvious influence on the WSS, compared to the gyroid and diamond strut topology. This information will enable an efficient estimate of the local WSS by using graded scaffolds for *in vitro* mechanobiological experiments. This will also facilitate the prediction of cellular responses with reference to specific mechano-regulation theory for different mechanobiological applications.

The permeability of graded scaffolds shows anisotropic properties,

Table 2
Relationship between local WSS and position in porosity gradient direction (x direction) based on linear regression.

Linear regression for geometries with gradual porosity: $\tau = p_1 \cdot x + p_2$

τ = average wall shear stress [Pa], x = x spatial coordinate corresponding to the changing in porosity direction [m]

	90 – 80%∥	90 – 80%⊥	80 – 70%∥	80 – 70%⊥	70 – 60%∥	70 – 60%⊥	90 – 70%∥	90 – 70%⊥	80 – 60%∥	80 – 60%⊥	90 – 60%∥	90 – 60%⊥
Gyroid Structure												
p_1	0.3377	−0.107	0.4741	−0.1401	0.7052	−0.2361	0.7596	−0.2709	1.121	−0.4045	1.396	−0.5004
p_2	0.007946	0.01076	0.009642	0.01334	0.01195	0.01721	0.007698	0.01239	0.00917	0.01573	0.007079	0.01428
Schwarz Structure												
p_1	0.1073	−0.05826	0.08494	−0.09396	−0.5505	−0.5505	0.369	−0.2472	0.5293	−0.4869	0.8782	−0.4597
p_2	0.006883	0.006479	0.008514	0.008498	0.01294	0.01294	0.00695	0.007809	0.008685	0.01094	0.006704	0.009365
Diamond Structure												
p_1	0.4433	−0.1629	0.7165	−0.2638	0.7203	−0.3187	1.124	−0.4504	1.457	−0.6068	1.847	−0.784
p_2	0.01054	0.01275	0.01294	0.01633	0.01725	0.02081	0.01002	0.01498	0.01254	0.01899	0.009508	0.01737

and this anisotropic property is more obvious with the increase of porosity gradient as shown in Fig. 4b. For example, the graded Schwarz strut topology scaffold (porosity = 90 %–80 %) has the permeability difference of 2.4 % in the directions of parallel and perpendicular with the porosity gradient direction. When porosity difference increases to 60 %–90 %, the permeability difference increases to 31 %. In addition, previous study reported that for trabecular bone – like structures (porosity ≈ 80 %), the difference of permeability in different directions can be in the range of 4.2 %–18.4 % [13]. This is within the range of permeabilities' anisotropy of the present study. To correlate the permeability (κ) with average WSS (τ_a) within scaffolds, another previous study reported an empirical model [20]:

$$\frac{\tau_a}{V_{in}} = 0.002116 \bullet \kappa^{-0.4793} \tag{9}$$

where, V_{in} is the inlet fluid velocity.

Applying this empirical model to the graded scaffolds the present study obtains an average WSS of 11.6 mPa for the scaffolds with graded porosities of 80 %–60 %, which have the permeability of 1.58×10^{-8} m^2 (Fig. 4b). In the CFD simulation, the average WSS is 10.9 mPa for this scaffold (Fig. 4a), so, the difference of average WSS is 11.6 mPa [20] vs 10.9 mPa (this study) which is small. Therefore, with the known scaffold permeability, to estimate the average WSS within graded scaffolds without performing CFD simulation, the empirical model proposed by Ahmed et al. [20] could be used. However, more verification is needed to assess the accuracy of using the empirical model by Ahmed et al. [20] for predicting the WSS within different types of graded scaffolds.

3.2. Case study: application to bone tissue engineering in vitro

If the scaffold is applied in mechanobiology study for bone tissue engineering *in vitro*, according to the previous mechano-regulation theory for bone tissue engineering *in vitro* [4], we find that the direction of the flow (parallel/perpendicular to the porosity gradient) has no influence on the struts area fraction for different mechanobiological responses such as osteogenic differentiation w/o mineralization, within the scaffolds that have a graded porosity of 90 %–70 % (see Fig. 5). This indicates that it is unnecessary to consider how to place the graded scaffolds within the perfusion bioreactor in 3D mechanobiological studies for *in vitro* bone tissue engineering under low applied flow velocity (such as: 1.0 mm/s), even though the graded scaffolds have anisotropic properties in terms of WSS and permeability. Nevertheless, considering the factors that can influence the WSS distribution, such as porosity gradient and applied flow velocity, for different *in vitro* applications, the mechanobiological responses might be influenced more significantly by graded porosity if higher porosity gradients and higher flow velocities are used.

The major limitations in this study are that the applied flow was in one direction (in steady state) and only one type of graded porosity was tested in the application of bone tissue engineering. However, other studies have shown that the flow direction would also influence the cellular responses in bone tissue engineering [21]. In the future, a more comprehensive mechano-regulation theory will need to be established for bone tissue regeneration by considering the influence of time-dependent direction change of flow/shear stress. In this case study, it was sought to test the anisotropic/isotropic properties of graded scaffold in terms of WSS for stimulating osteogenesis. To investigate the influence of porosity graded on mechanobiological responses for bone tissue engineering, a comprehensive study, which covers different porosity gradients will be needed.

4. Conclusion

In this study, it has been found that the porosity gradient of TPMS scaffolds has distinct influence on their internal WSS and overall
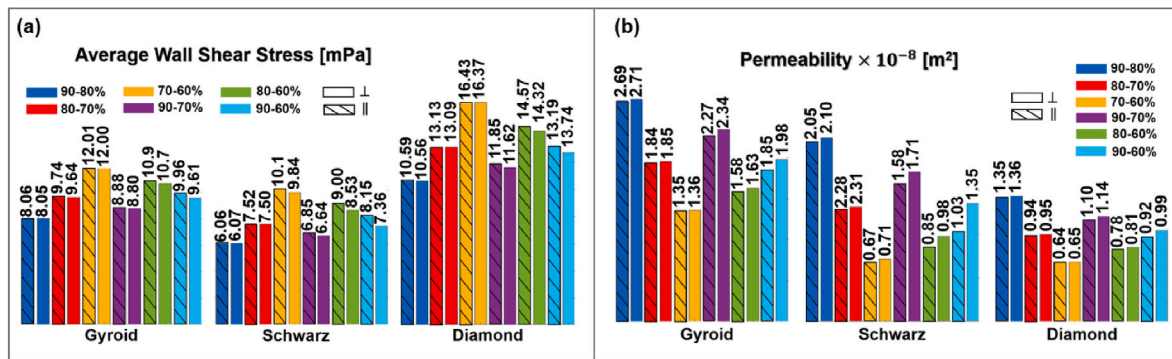
Fig. 4. (a) Average WSS within graded scaffolds, **(b)** permeability of scaffolds with graded porosities. ⊥: flow perpendicular to the porosity gradient direction; ‖: flow parallel to the porosity direction.
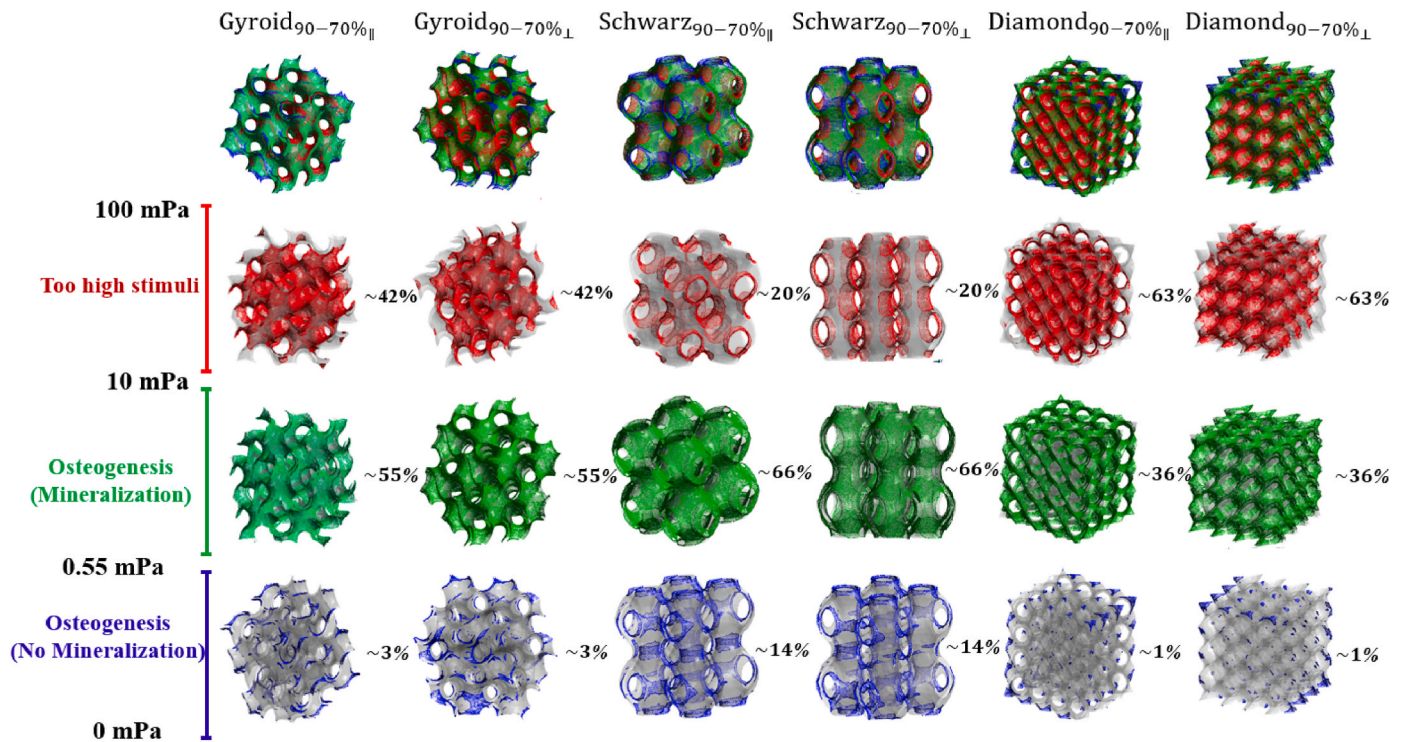

Fig. 5. Prediction of the scaffolds (graded porosity = 70 %–90 %) areas that have different mechanobiological responses in bone tissue engineering *in vitro* under parallel (‖) and perpendicular (⊥) flows. Here assumption is made that cells are flatly attached on the strut surfaces, and the WSS on cells is identical to the WSS on the struts wall. WSS ranges for different cell responses in bone tissue engineering *in vitro* is based on [4].

permeability. The WSS distribution along the direction of porosity gradient is dependent on the porosity gradient (porosity difference = 10 %–30 %), strut topology and flow direction. Furthermore, the influence of porosity gradient on the local WSS was quantified. Secondly, the graded scaffolds show the anisotropic properties in terms of overall average WSS (up to 11 % difference) and permeability (up to 31 % difference). This information provides guidance for addressing important practical issues within 3D mechanobiological/tissue engineering experiments via improving the design of graded TPMS and/or optimization of placement and application of graded scaffolds within bioreactors.

CRediT authorship contribution statement

Chiara Angela De Rosa: Writing – original draft, Visualization, Software, Methodology, Investigation, Funding acquisition, Formal analysis, Data curation. **Christopher J. Wright:** Writing – review & editing, Conceptualization. **Yi Xiong:** Conceptualization. **Francesco Del Giudice:** Writing – review & editing, Supervision, Conceptualization. **Feihu Zhao:** Writing – review & editing, Writing – original draft, Supervision, Conceptualization.

Declaration of competing interest

The authors declare no conflict of interest involved in this study.

Acknowledgement

Appendix A. Supplementary data

Supplementary data to this article can be found online at https://doi.org/10.1016/j.compbiomed.2025.109674.

References

[1] S. Kim, M. Uroz, L.J. Bays, C. Chen, Harnessing mechanobiology for tissue engineering, Dev. Cell 56 (2) (2021) 180–191, https://doi.org/10.1016/j.devcel.2020.12.017.

[2] S.M. Naqvi, L.M. McNamara, Stem cell mechanobiology and the role of biomaterials in governing mechanotransduction and matrix production for tissue regeneration, Front. Bioeng. Biotechnol. 8 (December) (2020) 1–27, https://doi.org/10.3389/fbioe.2020.597661.

[3] R.M. Delaine-Smith, G.C. Reilly, Mesenchymal stem cell responses to mechanical stimuli, Muscles, Ligament Tendons J. 2 (3) (2012) 169–180.

[4] J. Melke, F. Zhao, B. van Rietbergen, K. Ito, S. Hofmann, Localisation of mineralised tissue in a complex spinner flask environment correlates with predicted wall shear stress level localisation, Eur. Cell. Mater. 36 (2018) 57–68, https://doi.org/10.22203/eCM.v036a05.

[5] C. Bacci, V. Wong, V. Barahona, N. Merna, Cardiac and lung endothelial cells in response to fluid shear stress on physiological matrix stiffness and composition, Microcirculation 28 (1) (2021), https://doi.org/10.1111/micc.12659.

[6] T. Yi, S. Huang, G. Liu, T. Li, Y. Kang, Y. Luo, J. Wu, Bioreactor synergy with 3D scaffolds: new era for stem cells culture, ACS Appl. Bio Mater. 1 (2) (2018) 193–209, https://doi.org/10.1021/acsabm.8b00057. American Chemical Society.

[7] F. Zhao, Y. Xiong, K. Ito, B. van Rietbergen, S. Hofmann, Porous geometry guided micro-mechanical environment within scaffolds for cell mechanobiology study in bone tissue engineering, Front. Bioeng. Biotechnol. 9 (September) (2021) 1–10, https://doi.org/10.3389/fbioe.2021.736489.

[8] Z. Dong, X. Zhao, Application of TPMS structure in bone regeneration, Eng. Regenert. 2 (2021) 154–162, https://doi.org/10.1016/j.engreg.2021.09.004.

[9] T. Pires, J.W.C. Dunlop, P.R. Fernandes, A.P.G. Castro, Challenges in computational fluid dynamics applications for bone tissue engineering, Proc. R. Soc. A 478 (2257) (2022), https://doi.org/10.1098/rspa.2021.0607.

[10] A.A. Zadpoor, Additively manufactured porous metallic biomaterials, J. Mater. Chem. B 7 (26) (2019), https://doi.org/10.1039/c9tb00420c.

[11] F.P.W. Melchels, B. Tonnarelli, A.L. Olivares, I. Martin, D. Lacroix, J. Feijen, D.J. Wendt, D.W. Grijpma, The influence of the scaffold design on the distribution of adhering cells after perfusion cell seeding, Biomaterials 32 (11) (2011) 2878–2884, https://doi.org/10.1016/j.biomaterials.2011.01.023.

[12] H. Seddiqi, A. Saatchi, G. Amoabediny, M.N. Helder, S. Abbasi Ravasjani, M. Safari Hajat Aghaei, J. Jin, B. Zandieh-Doulabi, J. Klein-Nulend, Inlet flow rate of perfusion bioreactors affects fluid flow dynamics, but not oxygen concentration in 3D-printed scaffolds for bone tissue engineering: computational analysis and experimental validation, Comput. Biol. Med. 124 (2020), https://doi.org/10.1016/j.compbiomed.2020.103826.

[13] C. Karuna, T. Poltue, S. Khrueaduangkham, P. Promoppatum, Mechanical and fluid characteristics of triply periodic minimal surface bone scaffolds under various functionally graded strategies, J. Comput. Design Eng. 9 (4) (2022) 1258–1278, https://doi.org/10.1093/jcde/qwac052.

[14] F. Zhao, J. Melke, K. Ito, B. van Rietbergen, S. Hofmann, A multiscale computational fluid dynamics approach to simulate the micro-fluidic environment within a tissue engineering scaffold with highly irregular pore geometry, Biomech. Model. Mechanobiol. 18 (6) (2019) 1965–1977, https://doi.org/10.1007/s10237-019-01188-4.

[15] I. Maskery, L. Sturm, A.O. Aremu, A. Panesar, C.B. Williams, C.J. Tuck, R.D. Wildman, I.A. Ashcroft, R.J.M. Hague, Insights into the mechanical properties of several triply periodic minimal surface lattice structures made by polymer additive manufacturing, Polymer 152 (2018) 62–71, https://doi.org/10.1016/j.polymer.2017.11.049.

[16] F. Zhao, B. van Rietbergen, K. Ito, S. Hofmann, Flow rate in perfusion bioreactor to maximise mineralization in bone tissue engineering in vitro, J. Biomech. 79 (2018) 232–237, https://doi.org/10.1016/j.jbiomech.2018.08.004.

[17] A.P.G. Castro, T. Pires, J.E. Santos, B.P. Gouveia, P.R. Fernandes, Permeability versus design in TPMS scaffolds, Materials 12 (8) (2019), https://doi.org/10.3390/ma12081313.

[18] X.Y. Zhang, G. Fang, S. Leeflang, A.A. Zadpoor, J. Zhou, Topological design, permeability and mechanical behavior of additively manufactured functionally graded porous metallic biomaterials, Acta Biomater. 84 (2019) 437–452, https://doi.org/10.1016/j.actbio.2018.12.013.

[19] N. Annabi, J.W. Nichol, X. Zhong, C. Ji, S. Koshy, A. Khademhosseini, F. Dehghani, Controlling the porosity and microarchitecture of hydrogels for tissue engineering, Tissue Eng., Part B 16 (4) (2010) 371–383, https://doi.org/10.1089/ten.teb.2009.0639.

[20] H. Ahmed, M. Bedding-Tyrrell, D. Deganello, Z. Xia, Y. Xiong, F. Zhao, Efficient calculation of fluid-induced wall shear stress within tissue engineering scaffolds by an empirical model, Med. Novel Tec. Devices 18 (2023), https://doi.org/10.1016/j.medntd.2023.100223.

[21] Nile, M., Folwaczny, M., Wichelhaus, A., Baumert, U. & Rankovic, M. J. Fluid flow shear stress and tissue remodeling – an orthodontic perspective: evidence synthesis and differential gene expression network analysis. Front. Bioeng. Biotechnol., 11 (September), 1-26. https://doi.org/10.3389/fbioe.2023.1256825.